

STELLAR-AIDED INERTIAL NAVIGATION SYSTEMS FOR LUNAR AND MARS EXPLORATION

LT Benjamin P. Malay
U.S. Navy

Dr. David Gaylor and Dr. George Davis
Emergent Space Technologies, Inc

ABSTRACT

Accurate, robust navigation for the exploration of the Moon and Mars is required for a variety of applications, including manned and unmanned lander descent/ascent, landing site survey/registration, and surface operations. In this paper, we examine the use of a stellar-aided inertial navigation system (SAINS) for use on the surface of the Moon and Mars. The goal is to show that SAINS can enable global, continuous, autonomous navigation for surface vehicles (landers, rovers or aircraft) and astronauts.

The theory and SAINS model were originally developed for a study of Mars celestial navigation and will be presented as such. The lunar results are based on a model developed with the same theory which included the more complex rotational dynamics of the Moon. An extended Kalman filter was used to process simulated star position measurements to provide high-accuracy navigation solutions. High-fidelity models of the planetary environments and inertial measurement unit (IMU) were employed. The results were verified by a Monte Carlo analysis, and the predominant sources of error were identified with an error budget.

It is shown that a SAINS can achieve accuracies of approximately 300 *m* on Mars and 400 *m* on the Moon with a high quality IMU. Although the Moon lacks an atmosphere and has a smaller radius than Mars, the larger ratio of the IMU accelerometer bias to the surface gravity accounts for the less accurate results on the Moon. This paper has many applications to lunar surface navigation in support of the Robotic Lunar Exploration Program.

INTRODUCTION

The United States and its international aerospace partners are considering an expanding lunar and Mars exploration program over the coming decades. Robotic rovers that can traverse increasingly longer distances are critical to this program. With increased mobility comes a greatly increased science return for the same investment. A rover can sample many sites, autonomously search for geological and possible biological treasure troves, and explore areas with terrain too rugged to safely land in. However, one of the fundamental technologies that must be advanced to fully exploit such capabilities is autonomous surface navigation.

As the mission goals become more complex and the rover more autonomous, the navigation system performance must increase in accuracy and reliability. An ideal navigation system design must also take into account the hardware on the surface element as well as the supporting infrastructure, whether it be in orbit around the Moon, Mars or back on Earth.

Celestial navigation can likely fulfill nearly every navigation requirement for a surface vehicle (lander, rover, or aircraft) with no infrastructure required. In most cases, the surface vehicle will already have a strapdown IMU, and the only additional equipment required is a star camera and clock. Celestial navigation is simple, accurate, reliable, inexpensive, practically independent of all external inputs, and can be made autonomous.

The general SAINS formulation is derived and documented in Kayton,¹ Lin,² and Pitman.³ The performance of a terrestrial strapdown SAINS is analyzed by Levine.⁴ This paper presents the underlying dynamics and a discussion of a celestial navigation simulation developed for use on the Moon and Mars. The lack of published studies in this field is not because a SAINS would not perform well on other planetary surfaces. It is more likely because most engineers are unfamiliar with celestial navigation or have a perception that such technology is outdated. However, this perception is uninformed, and overlooking celestial navigation eliminates a practical solution that can be readily implemented for exploration systems.

SYMBOLS

ϕ	Latitude
λ	Longitude
h	Height above the reference ellipsoid
\mathbf{a}	True acceleration vector
\mathbf{a}^m	Measured acceleration vector
Υ_a	Accelerometer non-orthogonality matrix
Ξ_a	Accelerometer scale factor matrix
\mathbf{b}_a	Accelerometer bias errors
ϵ_a	Accelerometer white noise
$\mathbf{V}_a(t)$	Accelerometer white noise intensity
Ω_{ic}	True angular velocity of case frame wrt inertial space in case frame coordinates
Ω_{ic}^m	Measured angular velocity of case frame wrt inertial space in case frame coordinates
Υ_g	Gyro non-orthogonality matrix
Ξ_g	Gyro scale factor matrix
\mathbf{b}_g	Gyro bias errors
ϵ_g	Gyro white noise
$\mathbf{V}_g(t)$	Gyro white noise intensity
\mathbf{s}_m	Unit vector to a star in MCMF frame
\mathbf{y}_s	Measured unit vector to a star in case frame
\mathbf{s}_c^m	Measured unit vector to a star in case frame
Υ_s	Star sensor non-orthogonality matrix
Ξ_s	Star sensor scale factor matrix
\mathbf{b}_s	Star sensor bias errors
ϵ_s	Star sensor white noise
$\mathbf{R}_s(t)$	Star sensor white noise intensity
y_h	Barometric altitude measurement
y_v	Scalar velocity update
\mathbf{Q}	Attitude quaternion

THEORY

The coordinate frames, instrument models, and process model used in this study are presented in this section. Emphasis is placed on Mars, but it is clear that the concepts are directly applicable to lunar navigation.

Coordinate Frames

When star observations are used to determine position, the INS must be mechanized in a locally level frame. Celestial navigation works because a position estimation error will result in a change of the predicted position of a star. For locally level mechanizations, the frame itself rotates with a position error. The star observation is relative to the locally level frame, so the star's predicted position will rotate with it. This section defines all of the coordinate frames used in the SAINS mechanization.

Inertial Frames

The foundation of all reference frames used in this study is the J2000.0 system. The other important inertial coordinate frame is the Mars-centered Mars Mean Equator (or Moon-centered Moon Mean Equator) and International Astronomical Union (IAU)-vector of Date. It is also referred to as the Mars (or Moon) Centered Inertial (MCI) frame. This frame uses the rotational axis of Mars (or the Moon) as the z -axis, making the equatorial plane the reference plane. The IAU-vector, the x -axis, is a vector along the intersection of the Mars Mean Equator of Date (or Moon Mean Equator of Date) and the Earth Mean Equator of epoch 2000.0 reference planes. The MCI frame is denoted by the subscript i in mathematical formulas.

Central Body Rotating Frame

The central body rotating frame, also referred to as the Mars Centered Mars Fixed (MCMF) or Moon Centered Moon Fixed frame, is defined by the rotational axis of the central body as the z -axis and the intersection of the prime meridian and the equator as the x -axis. The MCMF frame is aligned with the MCI frame, but rotates about their common z -axis at the rotation rate of the Mars (or the Moon). This frame is denoted by the subscript m in mathematical formulas.

Locally Level Frame

The SAINS is mechanized in a locally level frame based on a standard reference ellipsoid as defined in Seidelmann.⁵ At any location on the planet, the x -axis points east, the y -axis points north, and the z -axis is normal to the ellipsoid and positive up. In this mechanization, position is given in geographic spherical coordinates: latitude (ϕ), longitude (λ), and height above the reference ellipsoid (h). The relationship between this frame and MCMF frame is shown in Figure 1. Velocity is given as cartesian velocity east, north, and up. The horizon plane of this frame is always tangent to the reference ellipsoid, hence the name. The locally level frame moves with the surface element as it traverses the planet and rotates with respect to the MCMF frame. The velocity state is the velocity of the frame itself. It must be understood that the areographic coordinates give the position of the surface element and the locally level frame tied to it, but the system is not mechanized in the MCMF frame. The locally level frame is denoted by the subscript l in mathematical formulas.

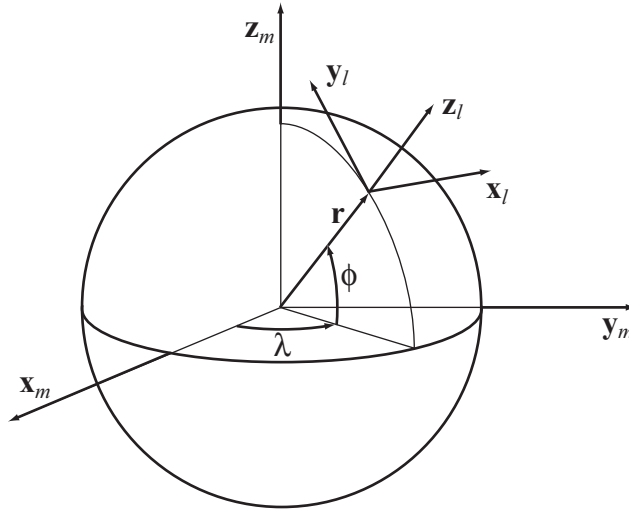


Figure 1 Locally Level Frame.

Case Frame

The case frame is defined by the accelerometer and gyroscope triad which is rigidly fixed to the frame of the vehicle in a strapdown system. Attitude, the orientation of the case frame with respect to the locally level frame, is maintained through a quaternion formulation. The case frame is denoted by the subscript c in mathematical formulas.

Mars and Moon Rotational Dynamics

Mars's rotational and orientation constants used in this study are found in the the most recent IAU/IAG Working Group on Cartographic Coordinates and Rotational Elements of the Planets and Satellites.⁵ Mars precession is only considered in the transformation between the J2000.0 and MCI frames. The effects of nutation are less than 1 arc-second (1 as). All rotational and orientation constants are considered to be known exactly *a priori*. This assumption is valid. Malay⁶ has further discussion.

The model for the lunar rotational dynamics is also found in Seidelmann⁵ and includes the periodic terms for precession and nutation. The nutation is much larger in magnitude for the Moon than for Mars, on the order of 10 arc-minutes. Ignoring this motion for the Moon would result in large position errors. The more complex rotation model is used in all transformations from the J2000.0 to the Moon-centered-inertial frame.

Gravity Models

Two different gravity models were used in this study. Gravity can be modelled as a vector normal to the reference ellipsoid using the formula of Somigliana, found in Heiskanen and Moritz.⁷ The actual gravity field of Mars is much more complex and must be modelled with a spherical harmonic function for realistic results. The coefficient set from the NASA Planetary Data System⁸ is nominally 85×85 , but using the entire set would be computationally excessive. In most cases, the spherical harmonic set has been truncated to 5×5 .

The *Arenautical Almanac*

Without an accurate star ephemeris, celestial navigation on the surface of Mars would not be possible. Malay created this ephemeris, the *Arenautical Almanac*, as part of a Trident research project while at the U.S. Naval Academy. The *Arenautical Almanac* is the ephemeris and algorithm that lists the positions of the navigable stars and planets in an areocentric reference frame. The almanac is mathematically accurate to 1 *as*, but no instruments accurate enough to physically confirm that figure have been landed on Mars. See Malay⁶ for a more detailed discussion.

The star ephemeris used for the lunar simulation includes a full precession and nutation model, and therefore has an accuracy significantly better than 1 *as*. However, the accuracy has not been determined mathematically, and therefore the lunar simulation conservatively uses 1 *as* stochastic errors as well.

Aided Inertial Navigation Systems

An unaided INS requires a precise initial alignment and position fix. Any errors in the initialization will grow over time. Even with perfect alignment, the position and velocity information will degrade as a result of unmodelled accelerations and instrument errors. With external measurements, errors inherent to an INS can be reduced to the accuracy of the external sensors and will remain bounded. In locally level INS mechanizations, the vertical channel is unstable, and the error grows rapidly. This error is eliminated by aiding the INS with barometric altitude data. Position and attitude errors can be reduced by such measurements as radio ranges, Doppler radar velocity updates, and star positions. Kalman filtering, one of the best methods to process measurements, is the approach used in the SAINS simulation.

IMU Error Model

The acceleration and angular velocity measured by the IMU are corrupted by several types of errors, both stochastic and systematic. The accuracy of the state estimate provided by the inertial navigation system is highly dependent on the magnitude of these instrument errors. The IMU error model used in the SAINS simulation is based on Maybeck¹⁰ and Savage.¹¹

Accelerometers and Gyroscopes

The accelerometers measure the nongravitational accelerations in case frame coordinates, denoted by \mathbf{a}^m . The measurement is corrupted by nonorthogonality errors, scale factor errors, biases, and noise. The equations of motion require the true accelerations, denoted by \mathbf{a} . The accelerometer error model is defined as

$$\mathbf{a}^m = (\mathbf{I} + \mathbf{\Upsilon}_a + \mathbf{\Xi}_a)(\mathbf{a} + \mathbf{b}_a + \boldsymbol{\epsilon}_a) \quad (1)$$

where

$$\mathbf{\Upsilon}_a = \begin{bmatrix} 0 & v_{a_{xz}} & -v_{a_{xy}} \\ -v_{a_{yz}} & 0 & v_{a_{yx}} \\ v_{a_{zy}} & -v_{a_{zx}} & 0 \end{bmatrix} \quad \mathbf{\Xi}_a := \begin{bmatrix} \xi_{a_x} & 0 & 0 \\ 0 & \xi_{a_y} & 0 \\ 0 & 0 & \xi_{a_z} \end{bmatrix} \quad \mathbf{b}_a := \begin{bmatrix} b_{a_x} \\ b_{a_y} \\ b_{a_z} \end{bmatrix} \quad (2)$$

and $\mathbf{v}_a = [v_{a_{xy}} v_{a_{xz}} v_{a_{yx}} v_{a_{yz}} v_{a_{zx}} v_{a_{zy}}]^T$ is the nonorthogonality error, $\boldsymbol{\xi}_a = [\xi_{a_x} \xi_{a_y} \xi_{a_z}]^T$ is the scale factor error, \mathbf{b}_a is the accelerometer bias, and $\boldsymbol{\epsilon}_a$ is a white noise stochastic process. The nonorthogonality errors, scale factor errors, and biases are modelled as zero-mean Gaussian random constants. The noise is modelled as a zero-mean, Gaussian-distributed, time uncorrelated random process with noise intensity $\mathbf{V}_a(t)$. The $\dot{\mathbf{r}}$ equation of motion requires the value of \mathbf{a} , which can be isolated from Equation 1 such that

$$\mathbf{a} = (\mathbf{I} - \boldsymbol{\Upsilon}_a - \boldsymbol{\Xi}_a)\mathbf{a}^m - \mathbf{b}_a \quad (3)$$

The noise is removed from Equation 3 because it is not known a priori and cannot be estimated. However, the simulated accelerometer measurements include stochastic errors.

The gyroscopes measure the angular velocity of the case frame relative to inertial space in case frame coordinates, denoted by $\boldsymbol{\Omega}_{ic}^m$. Similarly, the measurement is corrupted by nonorthogonality errors $\mathbf{v}_g = [v_{g_{xy}} v_{g_{xz}} v_{g_{yx}} v_{g_{yz}} v_{g_{zx}} v_{g_{zy}}]^T$, scale factor errors $\boldsymbol{\xi}_g = [\xi_{g_x} \xi_{g_y} \xi_{g_z}]^T$, biases \mathbf{b}_g , and noise $\boldsymbol{\epsilon}_g$. The equations of motion require the true angular velocity, denoted by $\boldsymbol{\Omega}_{ic}$. The gyroscope error model is defined as

$$\boldsymbol{\Omega}_{ic}^m = (\mathbf{I} + \boldsymbol{\Upsilon}_g + \boldsymbol{\Xi}_g)(\boldsymbol{\Omega}_{ic} + \mathbf{b}_g + \boldsymbol{\epsilon}_g) \quad (4)$$

where

$$\boldsymbol{\Upsilon}_g := \begin{bmatrix} 0 & v_{g_{xz}} & -v_{g_{xy}} \\ -v_{g_{yz}} & 0 & v_{g_{yx}} \\ v_{g_{zy}} & -v_{g_{zx}} & 0 \end{bmatrix} \quad \boldsymbol{\Xi}_g := \begin{bmatrix} \xi_{g_x} & 0 & 0 \\ 0 & \xi_{g_y} & 0 \\ 0 & 0 & \xi_{g_z} \end{bmatrix} \quad \mathbf{b}_g := \begin{bmatrix} b_{g_x} \\ b_{g_y} \\ b_{g_z} \end{bmatrix} \quad (5)$$

The $\dot{\mathbf{Q}}$ equation of motion requires the value of $\boldsymbol{\Omega}_{ic}$, which can be isolated from Equation 4 such that

$$\boldsymbol{\Omega}_{ic} = (\mathbf{I} - \boldsymbol{\Upsilon}_g - \boldsymbol{\Xi}_g)\boldsymbol{\Omega}_{ic}^m - \mathbf{b}_g \quad (6)$$

Again, the noise term has been removed as in the accelerometer error model, but is included in the simulated angular velocity measurements.

IMU Error Parameters

An IMU manufacturer provides data on the magnitude of the errors of a particular model based on experimental and operational testing. The error parameters for Gaussian random constants are the standard deviations (σ). The given parameter for the instrument noise is the intensity covariance ($\mathbf{V}/\Delta t$ where Δt is the integration step size). The specification lists for a Honeywell MIMU and a Litton LN100S are shown in Tables 1 and 2.

Accelerometer		Gyroscope	
Bias:	0.1 <i>mg</i>	Bias:	0.05°/ <i>hr</i>
Scale Factor:	175 <i>ppm</i>	Scale Factor:	5 <i>ppm</i>
Nonorthogonality:	14 <i>as</i>	Nonorthogonality:	25 <i>as</i>
Noise:	10 $\mu\text{g}/\sqrt{\text{Hz}}$	Noise:	0.01°/ $\sqrt{\text{hr}}$

Table 1 Honeywell MIMU Specifications.¹²

The equations of motions for all errors are simply $\dot{\mathbf{x}} = \mathbf{0} + \mathbf{w}_e$, where \mathbf{w}_e is a zero-mean white noise process with spectral density \mathbf{Q}_e . The process noise strength is very small and is scaled

Accelerometer		Gyroscope	
Bias:	0.025 <i>mg</i>	Bias:	0.001°/ <i>hr</i>
Scale Factor:	100 <i>ppm</i>	Scale Factor:	1 <i>ppm</i>
Nonorthogonality:	1 <i>as</i>	Nonorthogonality:	1 <i>as</i>
Noise:	5 $\mu g/\sqrt{\text{Hz}}$	Noise:	0.0006°/ $\sqrt{\text{hr}}$

Table 2 Litton LN100S Specifications.¹³

to the magnitude of the error. Its only purpose is to keep the Kalman gain for the error states from eventually going to zero. The position, velocity, and attitude states are augmented with the accelerometer and gyroscope errors in the filter model.

Observation Model

The inertial navigation system is aided with star observations, and this must be modelled in the SAINS filter. The *Arenautical Almanac* gives the position of a star as a unit vector in the MCMF frame at a given time, denoted by \mathbf{s}_m . The measurement, \mathbf{y}_s , is simply the position of the star relative to the case frame, \mathbf{s}_c^m . However, the measurement is corrupted by systematic and stochastic errors similar to the IMU error model. The position measured by the star sensor, \mathbf{s}_c^m , has biases, nonorthogonality, and scale factor errors such that

$$\mathbf{s}_c^m = (\mathbf{I} + \mathbf{\Upsilon}_s + \mathbf{\Xi}_s)(\mathbf{s}_c + \mathbf{b}_s) \quad (7)$$

where

$$\mathbf{\Upsilon}_s := \begin{bmatrix} 0 & v_{s_{xz}} & -v_{s_{xy}} \\ -v_{s_{yz}} & 0 & v_{s_{yx}} \\ v_{s_{zy}} & -v_{s_{zx}} & 0 \end{bmatrix} \quad \mathbf{\Xi}_s := \begin{bmatrix} \xi_{s_x} & 0 & 0 \\ 0 & \xi_{s_y} & 0 \\ 0 & 0 & \xi_{s_z} \end{bmatrix} \quad \mathbf{b}_s := \begin{bmatrix} b_{s_x} \\ b_{s_y} \\ b_{s_z} \end{bmatrix} \quad (8)$$

and $\mathbf{v}_s = [v_{s_{xy}} \ v_{s_{xz}} \ v_{s_{yx}} \ v_{s_{yz}} \ v_{s_{zx}} \ v_{s_{zy}}]^T$ is the northogonality error, $\boldsymbol{\xi}_s = [\xi_{s_x} \ \xi_{s_y} \ \xi_{s_z}]^T$ is the scale factor error, and \mathbf{b}_s is the star sensor bias. The nonorthogonality errors, scale factor errors, and biases are modelled as zero-mean Gaussian random constants. The star measurement is also corrupted by a zero-mean Gaussian white noise process \mathbf{u}_s of covariance \mathbf{R}_s . The state is augmented with the star sensor errors. The full star measurement model using input from the *Arenautical Almanac* is

$$\mathbf{y}_s = (\mathbf{I} + \mathbf{\Upsilon}_s + \mathbf{\Xi}_s)(\mathbf{T}_{lc}^T \mathbf{T}_{lm} \mathbf{s}_m + \mathbf{b}_s) + \mathbf{u}_s \quad (9)$$

The vertical channel of all locally level INS mechanizations is unstable and must be updated with barometric altitude measurements. The stochastic altitude measurement is modelled very simply as

$$y_h = h + u_h \quad (10)$$

A scalar velocity update can also be useful, especially a zero-velocity update for stationary vehicles. The measurement can readily be calculated from the rotation rate of the wheels. The stochastic velocity measurement is

$$y_v = \sqrt{v_x^2 + v_y^2 + v_z^2} + u_v \quad (11)$$

Process Model

The equations of motion in a locally level frame, IMU error models, and the observation model are summarized in this section. The augmented state is

$$\mathbf{x} = [\mathbf{r} \quad \mathbf{v} \quad \mathbf{Q} \quad \mathbf{b}_a \quad \mathbf{b}_g \quad \mathbf{b}_s \quad \boldsymbol{\xi}_a \quad \boldsymbol{\xi}_g \quad \boldsymbol{\xi}_s \quad \mathbf{v}_a \quad \mathbf{v}_g \quad \mathbf{v}_s]^\top \quad (12)$$

Position:

$$\begin{bmatrix} \dot{\phi} \\ \dot{\lambda} \\ \dot{h} \end{bmatrix} = \begin{bmatrix} 0 & \frac{1}{(R_m+h)} & 0 \\ \frac{1}{(R_p+h)\cos\phi} & 0 & 0 \\ 0 & 0 & 1 \end{bmatrix} \begin{bmatrix} v_x \\ v_y \\ v_z \end{bmatrix} \quad (13)$$

where R_m is the radius of curvature in the meridian direction and R_p is the radius of curvature in the parallel direction. The velocity $\mathbf{v} = [v_x \ v_y \ v_z]^\top$ is in local level coordinates. The definitions of the radius of curvature parameters are

$$R_m = \frac{a(1-e^2)}{(1-e^2\sin^2\phi)^{3/2}} \quad \text{and} \quad R_p = \frac{a}{(1-e^2\sin^2\phi)^{1/2}} \quad (14)$$

where

$$e = \frac{\sqrt{a^2 - b^2}}{a} \quad (15)$$

and a is the equatorial radius and b is the polar radius of the planet.

Velocity:

$$\begin{aligned} \dot{\mathbf{v}}_l &= \mathbf{g} - \mathbf{F}(\boldsymbol{\Omega}_{im})\mathbf{F}(\boldsymbol{\Omega}_{im})\mathbf{r}_l - \mathbf{F}(\boldsymbol{\Omega}_{ml} + 2\boldsymbol{\Omega}_{im})\mathbf{v}_l \\ &\quad + (\mathbf{I} - \boldsymbol{\Upsilon}_a - \boldsymbol{\Xi}_a)\mathbf{a}^m - \mathbf{b}_a + \mathbf{w}_v \end{aligned} \quad (16)$$

where the vector $\boldsymbol{\Omega} = [\Omega_x \ \Omega_y \ \Omega_z]^\top$ is the angular velocity of the rotating frame with respect to the inertial frame and

$$\mathbf{F}(\boldsymbol{\Omega}) := \begin{bmatrix} 0 & -\Omega_z & \Omega_y \\ \Omega_z & 0 & -\Omega_x \\ -\Omega_y & \Omega_x & 0 \end{bmatrix} \quad (17)$$

The angular velocities transformed into the proper coordinates are

$$\boldsymbol{\Omega}_{im} = \begin{bmatrix} 0 \\ \omega \cos \phi \\ \omega \sin \phi \end{bmatrix} \quad \text{and} \quad \boldsymbol{\Omega}_{ml} = \begin{bmatrix} \frac{-v_y}{(R_m+h)} \\ \frac{v_x}{(R_p+h)} \\ \frac{v_x}{(R_p+h)} \tan \phi \end{bmatrix} \quad (18)$$

where ω is the rotation rate of Mars. The equation for $\boldsymbol{\Omega}_{im}$ is the projection of ω in the locally level frame, and the equation for $\boldsymbol{\Omega}_{ml}$ comes from the definition $v = \Omega r$ in locally level coordinates. The term \mathbf{r}_l is the cartesian position vector from the center of Mars in locally level coordinates. It is equal to

$$\mathbf{r}_l = \begin{bmatrix} 0 \\ \frac{-ae^2}{\sqrt{1-e^2\sin^2\phi}} \cos\phi \sin\phi \\ a\sqrt{1-e^2\sin^2\phi} + h \end{bmatrix} \quad (19)$$

Attitude:

$$\dot{\mathbf{Q}} = \frac{1}{2} \mathbf{B}(\mathbf{Q}) [(\mathbf{I} - \Upsilon_g - \Xi_g) \Omega_{ic}^m - \mathbf{b}_g - \mathbf{T}_{lc}^T (\Omega_{im} + \Omega_{ml})] \quad (20)$$

where

$$\mathbf{B}(\mathbf{Q}) := \begin{bmatrix} q_4 & -q_3 & q_2 \\ q_3 & q_4 & -q_1 \\ -q_2 & q_1 & q_4 \\ -q_1 & -q_2 & -q_3 \end{bmatrix} \quad (21)$$

and the transformation matrix used to rotate from the case frame to the navigation frame is given by

$$\mathbf{T}_{lc} = \begin{bmatrix} 1 - 2(q_2^2 + q_3^2) & 2(q_1q_2 + q_3q_4) & 2(q_1q_3 - q_2q_4) \\ 2(q_1q_2 - q_3q_4) & 1 - 2(q_1^2 + q_3^2) & 2(q_2q_3 + q_1q_4) \\ 2(q_1q_3 + q_2q_4) & 2(q_2q_3 - q_1q_4) & 1 - 2(q_1^2 + q_2^2) \end{bmatrix} \quad (22)$$

Instrument Errors:

$$[\dot{\mathbf{b}}_a \quad \dot{\mathbf{b}}_g \quad \dot{\mathbf{b}}_s \quad \dot{\boldsymbol{\xi}}_a \quad \dot{\boldsymbol{\xi}}_g \quad \dot{\boldsymbol{\xi}}_s \quad \dot{\mathbf{v}}_a \quad \dot{\mathbf{v}}_g \quad \dot{\mathbf{v}}_s]^T = \mathbf{0} + \mathbf{w}_e \quad (23)$$

Initial Conditions:

$$\text{State Estimate:} \quad \hat{\mathbf{x}}_0 = \mathbf{x}_0 + \sigma_{\mathbf{x}} \text{randn} \quad (24)$$

$$\text{Covariance:} \quad \mathbf{P}_0 = \begin{bmatrix} \sigma_{x_1}^2 & 0 & 0 \\ 0 & \ddots & 0 \\ 0 & 0 & \sigma_{x_n}^2 \end{bmatrix} \quad (25)$$

RESULTS

To determine the feasibility of using a SAINS on the Moon and Mars, a simulation was constructed to perform the required numerical experimentation. The program simulates the planetary environment, a surface vehicle and IMU on the surface, a star sensor, and an extended Kalman filter to process the observations. A stationary vehicle was assumed. Proper filter performance was verified by a Monte Carlo analysis of the state estimates and covariance. The mean values of the estimation errors are zero and the square root of the covariance are equal to the standard deviations.

Figures 2 through 5 show the performance of a SAINS operating on the surfaces of the Moon and Mars with both a Honeywell MIMU-grade IMU and a Litton LN100S-grade IMU. The vehicles are stationary and located at 0° latitude with star observations taken every two seconds.

A lunar SAINS has an accuracy of approximately 1.4 km using a MIMU and 400 m using a LN100S. A SAINS on Mars has an accuracy of approximately 1.2 km with a MIMU and 300 m with a LN100S. The performance of the LN100S-grade IMU is clearly much better. This result is because the accelerometer biases of the LN100S almost an order of magnitude better than the MIMU unit. Accelerometer bias, whether it be from the IMU or errors in the gravity model, is by far the largest source of error in a SAINS.

A SAINS operating with a LN100S grade IMU may be accurate enough for autonomous guidance. If the accelerometer bias could be reduced by an order of magnitude through an additional measurement type, upgrading the IMU accelerometer, or various other methods, the total position error is reduced to 50 m as shown in Figure 6. This level of accuracy should allow global autonomous guidance. Research of methods to eliminate accelerometer biases from the measurements should be a high priority.

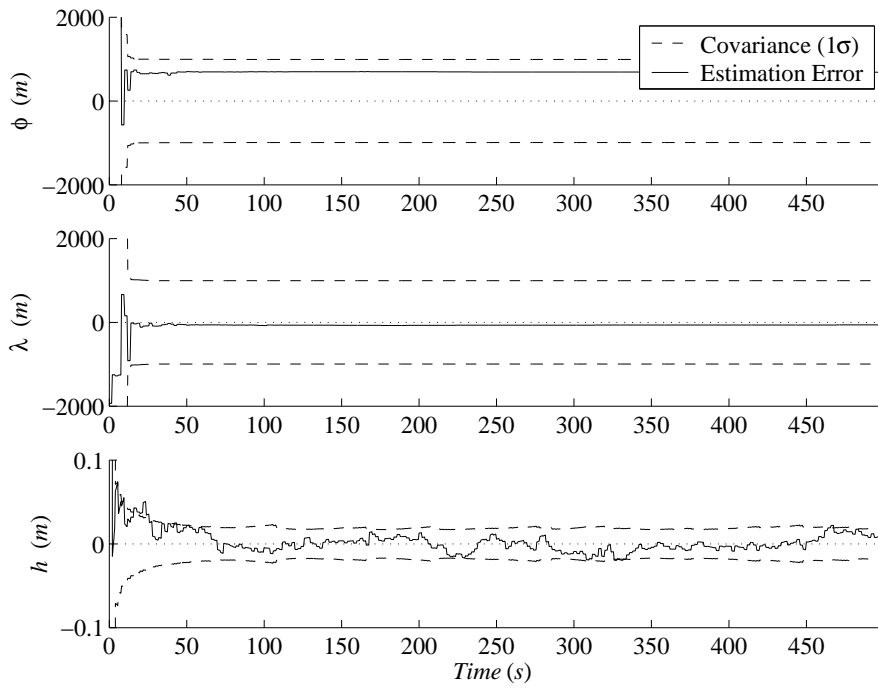


Figure 2 Moon Surface Vehicle, Honeywell MIMU - Position Errors.

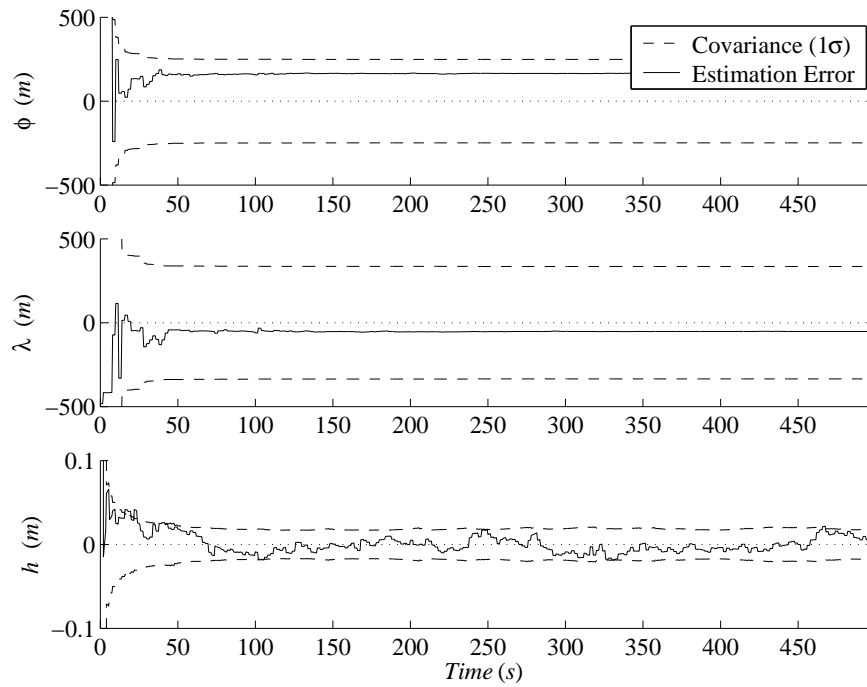


Figure 3 Moon Surface Vehicle, Litton LN100S - Position Errors.

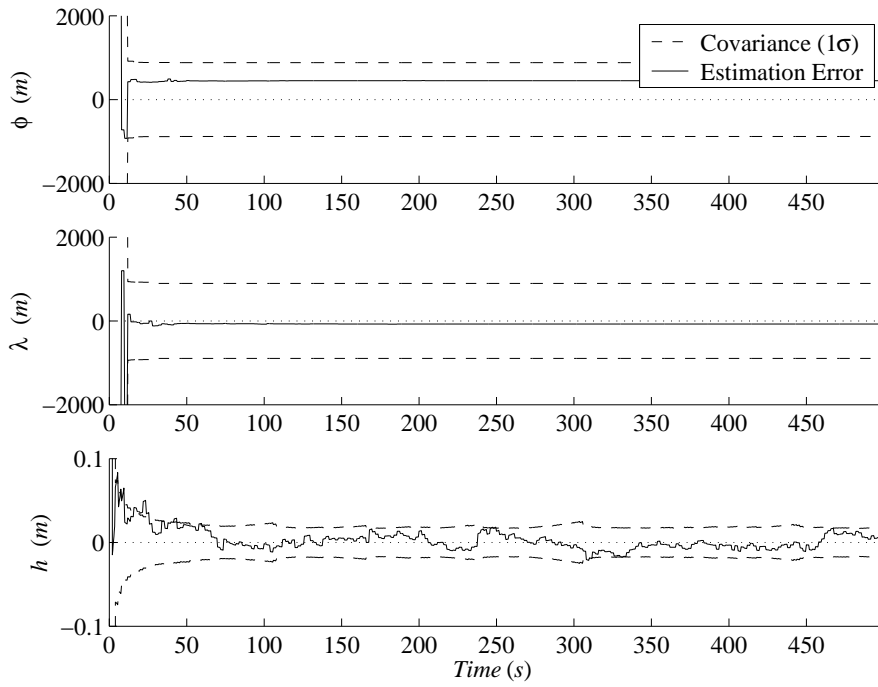


Figure 4 Mars Surface Vehicle, Honeywell MIMU - Position Errors.

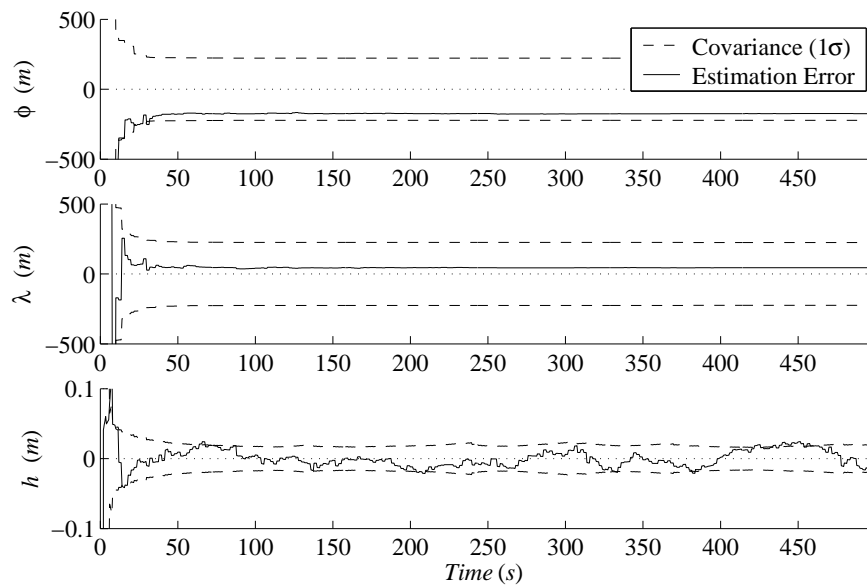


Figure 5 Mars Surface Vehicle, Litton LN100S - Position Errors.

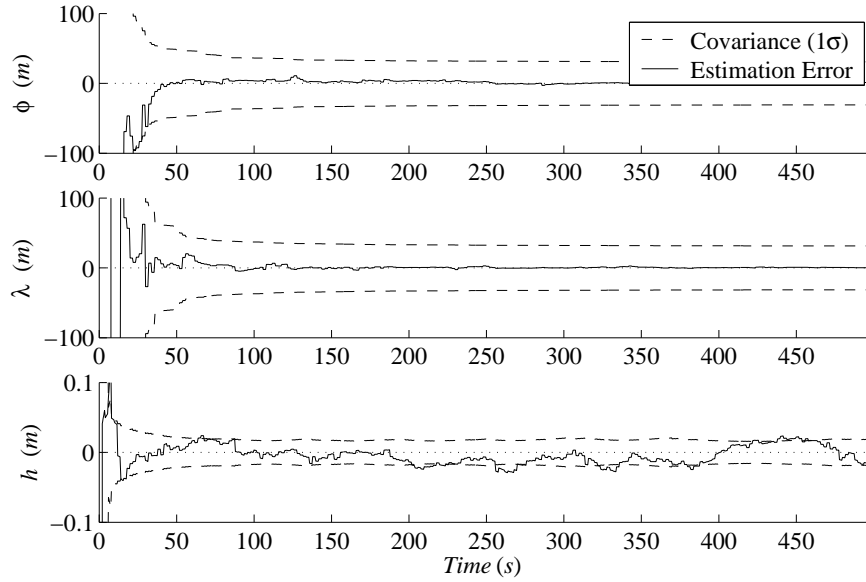


Figure 6 Litton LN100S, Accelerometer Bias Reduced.

Mars Error Budget

Even with a small accelerometer bias in the Litton LN100S, there is still a residual position estimation error. A simple error budget was performed to determine the percentage of the total error that each non-IMU error source contributes on Mars. The error sources considered in this error budget are the process noise, the star position measurement noise, the height measurement noise, and the total IMU instrument error. The optimal gain was stored from a run and the covariance values after 1000 s were used as the total error. The results of the position error budget are shown in Table 3.

Source	$\sigma_{\phi}^2 (rad^2)$	$\sigma_{\lambda}^2 (rad^2)$	$\sigma_h^2 (m^2)$
Q	2.7169×10^{-11}	1.2151×10^{-10}	1.8394×10^{-4}
R_s	8.1780×10^{-10}	8.0183×10^{-10}	3.4554×10^{-6}
R_h	8.7556×10^{-13}	4.7900×10^{-12}	7.0243×10^{-4}
IMU	1.0388×10^{-11}	1.4292×10^{-11}	1.2419×10^{-7}
Sum	8.5631×10^{-10}	9.4251×10^{-10}	8.9002×10^{-4}
Total	9.5905×10^{-10}	$1.0425e \times 10^{-9}$	8.8977×10^{-4}

Table 3 Mars Error Budget, Position.

Note that the sums of the error sources are not quite equal to the total error. This slight difference is a result of the nonlinear nature of the problem and possibly some correlations between the error sources. The error budget is useful for showing the relative contributions of the error sources. The following tables show the percentage of the total error that each source contributes.

Both the position errors stem predominantly from the star measurement noise and to a lesser degree the process noise. The results of this error budget show that the position estimation error of a SAINS for a given high-quality IMU is mostly driven by the star measurement noise.

Source	ϕ	λ	h
Q	2.8 %	11.7 %	20.7 %
R_s	85.3 %	76.9 %	0.4 %
R_h	0.1 %	0.5 %	78.9 %
IMU	1.1 %	1.4 %	0.0 %

Table 4 Mars Error Budget Percentage, Position.

CONCLUSIONS

The goals of this study were to show that celestial navigation can be used to find position on the surface of the moon and Mars and to determine the level of accuracy that can be expected. Until now, no studies have answered these questions. The most important conclusion is that celestial navigation can be used in the exploration of the Moon and Mars. With a Litton LN100S, the 1σ accuracy of a stellar-aided inertial navigation system on the Moon has a total position error of 400 *m* and on Mars has an accuracy of 300 *m* for the models considered. With accelerometer bias reduction methods, the accuracy can be increased substantially to approximately 50 *m*. This level of performance will allow global autonomous navigation.

Recommendations

The upcoming lunar and Mars surface vehicle designs will have an onboard IMU regardless of the external navigation system. Based on these results, the lander should use a Litton LN100S-grade IMU. However, the accelerometer bias of the unit should be reduced by an order of magnitude or estimated with other measurement types to realize the full potential of celestial navigation. If a star camera accurate to one arcsecond is added to the lander, it will make a complete navigation system independent of other infrastructure. The position errors are mostly a result of accelerometer biases, and the IMU should be chosen such that it minimizes the biases even at the expense of other errors. A SAINS must include a spherical harmonic gravity model or unacceptable position errors will result. The next largest source of error is the star measurement noise, which can only be reduced by updating the star ephemeris models.

Ground Control Network Surveying

A required component of a navigation satellite constellation is a ground control network used to update a satellite's ephemeris. The accuracy of the position fix from a satellite is only as accurate as the position estimates of the ground stations. Celestial navigation would be an excellent way to survey the ground control network. A global network of SAINS-equipped landers would also define a Moon or Mars-based reference frame relative to fixed inertial space and would be independent of any Earth-based frames. This is a necessary step of any long term exploration program. An accurate ground control network can also be used by spacecraft in the entry, descent, and landing phase for precision approaches. Additionally, data returned from SAINS ground stations could be used to update precession and nutation models and rotational rate values. This would increase the accuracy of the star ephemerides as well as be useful for planetary interior studies.¹⁴ Since satellite-based navigation will be the preferred navigation method on the Moon and Mars once the infrastructure is in place, the best long term application for celestial navigation may be as an interplanetary surveying tool.

Further Research

The results of this paper are very encouraging, but this is only one of many studies that must be performed before celestial navigation can be used on an operational mission. Presented here are issues that must be resolved before the SAINS can be taken from the theoretical to the operational environment.

- The dominant error source of a SAINS is the accelerometer bias. A study on methods to reduce or remove the bias from the IMU measurement would be the simplest way to increase the accuracy. This topic should be the highest priority of future SAINS research.
- An atmospheric refraction correction algorithm needs to be developed for Mars. All of the information required to perform this research is available, but it has not been done yet.
- The effect of dust on astronomic observations on Mars needs to be determined. The effect is most likely small, since high-resolution photographs of the surface are available.
- The bands of visible light that can be seen through the Mars atmosphere during the daytime need to be identified.
- This paper does not discuss star sensor design, and the instrument requirements need to be better defined. This includes field of view, magnitude limits, lens design, observation frequency, and other important considerations.
- The star catalogue used in the simulation is small, and the star identification and observation planning methods are rudimentary. This issue has already been resolved for terrestrial applications and simply needs to be included in the simulation.
- A SAINS would be a sizable subsystem on a robotic lander. The power, mass, and size budgets would have to be determined, including the influence on other subsystems.
- If a SAINS is used on a lander, it would affect the entire mission operation. Mission planners should find ways to maximize the benefits a SAINS provides, the most important being long-range autonomous roving. More sites could be visited in less time resulting in increased science return. A nuclear-powered surface vehicle would benefit most from the operational flexibility a SAINS can provide. While most of the operational effects would be positive, a surface vehicle would have to make periodic stops to reinitialize the SAINS.
- The extended Kalman filter in the SAINS simulation can process a number of other measurements besides star positions and barometric altitude. Ultra high-accuracy position estimates may be achieved by combining star measurements with electronic ranges from orbital and surface beacons. For aerial applications, doppler radar velocity measurements would also increase the accuracy of the position estimate.

Celestial navigation performed with a stellar-aided inertial navigation system is a viable method for surface navigation on the Moon and Mars. Now that it has been shown to work theoretically, the real work of turning it into an operational system can begin. Mission planners should not overlook this accurate and effective navigation method. As we continue to explore our planetary neighbors, celestial navigation will play an increasingly important role.

REFERENCES

1. Kayton, M. and Fried, W., *Avionics Navigation Systems*, Wiley, New York, 2nd ed., 1997.
2. Lin, C.-F., *Modern Navigation, Guidance, and Control Processing*, Prentice Hall, Englewood Cliffs, New Jersey, 1991.
3. Pitman, G., *Inertial Guidance*, Wiley, New York, 1962.
4. Levine, S., Dennis, R., and Bachman, K., "Strapdown Astro-Inertial Navigation the Optical Wide-Angle Lens Startracker," *Navigation*, Vol. 37, No. 4, Winter 1990-91.
5. Seidelmann, P., Abalakin, V., Bursa, M., Davies, M., De Bergh, C., Lieske, J., Obert, J., Simon, J., Standish, E., Stooke, P., and Thomas, P., "Report of the IAU/IAG Working Group on Cartographic Coordinates and Rotational Elements of the Planets and Satellites: 2000," *Celestial Mechanics and Dynamical Astronomy*, Vol. 82, 2002.
6. Malay, B. and Fahey, R., "Celestial Navigation on the Surface of Mars," *Advances in the Astronomical Sciences*, Vol. 112, 2002.
7. Heiskanen, W. and Moritz, H., *Physical Geodesy*, Freeman, San Francisco, 1967.
8. Simpson, R., editor, *MGS RST Science Data Products*, Vol. USA_NASA_JPL_MORS_1015, NASA Planetary Data System, 2001, See <http://pds-geophys.wustl.edu/pds/mgs/rs/> for latest data set.
9. Gelb, A., *Applied Optimal Estimation*, MIT Press, Cambridge, Massachusetts, 1974.
10. Maybeck, P., *Stochastic Models, Estimation, and Control*, Academic Press, Inc, Florida, 1997.
11. Savage, P., *Strapdown Analytics*, Strapdown Associates, Inc, Maple Plain, Minnesota, 2000.
12. Honeywell, *Miniature Inertial Measurement Unit (MIMU) Product Sheet*, 1999.
13. Litton, *LN-100S Gyro Reference Assembly*, 2001.
14. Folkner, W., Yoder, C., Yuan, D., Standish, E., and Preston, R., "Interior Structure and Seasonal Mass Redistribution of Mars from Radio Tracking of Mars Pathfinder," *Science*, Vol. 278, December 1997.